

Super Pressure Balloon Non-linear Structural Analysis and Correlation Using Photogrammetric Measurements

Joseph V. Welch*

ILC Dover LP, Frederica, Delaware, 19946

Shirong Wang†

TCOM LP, Columbia, Maryland, 21046

and

Joseph R. Blandino‡ and Kiley McEvoy§

James Madison University, Harrisonburg, Virginia, 22807

The structural analysis of high altitude scientific balloons is studied with the introduction of innovative experimental techniques. A bi-axial material test apparatus is investigated in order to provide a more complete definition of fabric material elongation properties. This fabric test device has been under development and a recent balloon material study has provided an excellent opportunity to evaluate its performance. Photogrammetric 3D shape measurements were conducted as part of a scale model balloon inflation test. Photogrammetry provides a full characterization of the 3D deformation under load so that a more rigorous evaluation of the Lagrangian strain tensor can be made. Pulling these two experimental efforts together, a finite element structural analysis of the balloon inflation test is presented. Material property inputs for the model were taken from both the uni-axial and bi-axial fabric testing. The 3D photogrammetry measurements were used to make detailed comparisons between the model response and that of the balloon experiment. The bi-axial test device was observed to under predict the actual stiffness at the initial points of the elastic modulus curve. At higher load states the bi-axial device provided fill direction modulus measurements that were in better agreement with the material stiffness observed during balloon inflation testing. A similar evaluation of the bi-axial warp modulus measurements was not possible with the range of loads that were measured. The increase in rigor, made possible by the Photogrammetry data, enabled a valuable evaluation the bi-axial fabric testing device.

Nomenclature

DP	=	inflation load increment
E_f	=	apparent Young's Modulus in material fill direction
E_w	=	apparent Young's Modulus in material warp direction
E_{AB}	=	Lagrangian strain tensor
L_T	=	distance between adjacent targets
R^2	=	variability in the response variable that is explained by regression
\mathbf{u}	=	displacement
\mathbf{x}	=	spatial coordinates

* Lead Analytical Engineer, Engineering Directorate, AIAA Senior Member.

† Senior Engineer, Engineering Department.

‡ Associate Professor, Integrated Science and Technology, MSC 4310, AIAA Senior Member.

§ Undergraduate Research Assistant, Integrated Science and Technology, MSC 4310.

\mathbf{X}	=	material coordinates
x	=	mapping from \mathbf{X} -> \mathbf{x}
ΔL_T	=	change in length from the baseline
ε_f	=	strain in material fill direction
ε_T	=	strain between target and adjacent targets
ε_w	=	strain in material warp direction
ν_{fw}	=	Poisson's ratio, - $\varepsilon_w / \varepsilon_f$ due to σ_f applied only
ν_{wf}	=	Poisson's ratio, - $\varepsilon_f / \varepsilon_w$ due to σ_w applied only
σ_f	=	stress in material fill direction
σ_w	=	stress in material warp direction

I. Introduction

TECHNOLOGY endeavors of the NASA Balloon Program have focused on factors enabling increases to the capability of scientific balloon missions. Balloon program performance goals call for 6000lb suspended loads at 110,000 ft, resulting in volumes of 22 million cubic feet. The NASA Ultra Long Duration Balloon program was initiated in 1997. The pumpkin style lobed super pressure design was conceived which has continued in development and test as NASA's selection for meeting these goals.

In 2004, a project was funded to investigate an alternative to the current pumpkin style design. The Alternative ULDB concept was a spherical super pressure envelope using a traditional gore method shown in Fig. 1. The material class under investigation was a lightweight woven polyester fabric. New technology components for this project were the implementation of innovative test methods and analytical structural modeling. A recently implemented fabric Bi-axial test method was used to develop mechanical property inputs necessary for structural analysis. A scale model test program was undertaken, where photogrammetry was used to take detailed 3D measurements for tested versus analytically predicted shape comparisons.

II. Background

A. Bi-axial Fabric Testing

One frequently used method for testing the elongation of fabric materials only pulls thin strips of fabric in one direction. This test is known as the Uni-axial Strip Tensile Test. A draw back to the Uni-axial strip tensile test is the transverse yarns have the tendency to be pushed out of the way as the axial yarns elongate under load.¹ This crimp interchange effect is shown in Fig. 2. While in use, inflatable softgoods products typically have the fabric material being loaded in multiple directions, creating the need for fabric mechanical properties under bi-axial load states. Cruciform loading fixtures have been used in that past for bi-axial loading of fabrics, especially in the tensile structure industry. An innovative bi-axial cruciform sample loading apparatus was designed and fabricated as part of a sponsored project for the 2002 University of Delaware Senior Design competition. This device is installed in the Instron Laboratory at ILC Dover.

B. Photogrammetry

Photogrammetry is an optical measurement technique that has been used to characterize the static shape of membrane and inflatable structures.²⁻⁶ By triangulating from known camera positions to the location of identical targets on a series of photographs, a three dimensional model of an imaged surface can be obtained. The imaged targets are usually circular and are either projected or physically attached to the surface of the structure. Projected targets have the advantage of not altering the surface of the structure, but the structure can move independently of the projected targets. Fixed targets add mass and local stiffness to the structure, but they move with the structure so changes in the relative position of the targets can be used to determine the strain. Recently, photogrammetry was used to measure bi-axial strain in an inflated cylinder with application to scientific balloons.⁷

C. Analytical Modeling

Structural analysis of softgoods inflated structures has presented some key challenges, and several techniques have been used in the past. A variational formulation has been used in the structural analysis of balloon shapes, including the ULDB pumpkin design.⁸⁻⁹ Specially developed in-house finite element analysis codes, such as the Goodyear Shell program have played important roles. Commercial finite element analysis programs have not only been applied to the balloon area, but also to areas where attributes of the fabric material architecture are important.¹⁰⁻

¹¹ In some softgoods finite element analysis cases, characteristics of the fabric material response make necessary the use of user defined material models.¹²⁻¹³

Several fabric modeling difficulties typically need to be addressed in structural analysis. Models with very thin membrane elements can often fail to reach a converged solution. The combination of orthotropic and non-linear elastic material properties presents a unique challenge for the analysis model. Material models such as multi-linear elastic from ANSYS can capture characteristics of the nonlinear material behavior, but can only be used for isotropic materials. The fabric material option in LS-DYNA can be used where both orthotropic and non-linear behaviors need to be included.

III. Current Study

A. Bi-axial Fabric Testing

Material property testing was conducted to determine best estimates for the material inputs required for the structural models. In this work elastic modulus, shear modulus and Poisson's ratio were estimated. For the scale model test program, 3 meter diameter test spheres were inflation tested. The test articles were constructed with a lightweight polyester material with a warp yarn count of 101 and a fill yarn count of 70. The material had a 0.5 mil Mylar coating on one side and a finished weight of 2.38 oz/yd². Uni-axial strip tensile testing was conducted for ten samples. Five each samples in the warp and five each in the fill direction were tested. The uni-axial data was measured as a baseline for comparison with the subsequent bi-axial measurements. The uni-axial Instron testing was conducted with preload cycling and at both 30.5 cm/min and 5.1 cm/min Instron head speeds. Test sample extension was recorded with a 1-inch extensometer.

Bi-axial testing was conducted for two cruciform samples of the material as shown in Fig. 3. A third sample was prepared but failed during Instron testing. In order to obtain a uniform stress distribution at the center region of cruciform sample, leg slitting was performed on each sample. Before bi-axial tensile testing, each sample was pre-loaded in warp and fill directions ten times, respectively. The pre-loads applied were 26.3 N/cm in warp and 21.9 N/cm in fill. A warp to fill load ratio of 1:1 was used for this testing due to the spherical geometry of the inflatable test article. The design model for the bi-axial loading device is shown in Fig. 4. The bi-axial test setup is shown in Fig. 5 and 6. Strain measurements were recorded using two one inch extensometers aligned with the warp and fill yarn directions. With the bi-axial test fixture, the vertical load is controlled and recorded through the Instron device. Horizontal load is applied to the sample by two pneumatic cylinders positioned by the trellis frame on linear bearings. Horizontal load is held at a constant value while the vertical loading changes. Both of the cruciform samples were tested twice, once with varying load in the warp direction and once with varying load in the fill direction.

Shear modulus for the material was determined with an inflated cylinder torsion test. The test setup for the shear modulus test is shown in Fig. 7. Two samples were tested. One sample had warp in axial direction and fill in hoop direction and the other vice versa. During the test, different inflation pressures (3.45, 6.9, 10.35, and 13.8 KPa) were applied to each sample to see the influence of inflation pressure on fabric shear stiffness. Torque was manually applied to the sample with a torque wrench and angular change of the cylindrical sample was measured.

B. Photogrammetry

For this investigation images from four 5.0 megapixel cameras were used in the photogrammetric analysis to measure the shape of the section of the balloon. One hundred and thirty 3.2 mm dia. retro-reflective targets were attached to the balloon's surface. The majority of the targets were arranged within a single gore with additional targets positioned to measure the balloon circumference at 90° to the gore centerline. The targets had a horizontal spacing of approximately 130 mm while the vertical spacing ranged from approximately 60 to 140 mm. Because of the small size of the targets and spacing, the targets added minimal mass to the balloon skin and any local stiffness caused by the targets was negligible. The balloon with targets attached is shown in Fig. 8. The cameras were set-up as shown in Fig. 9. The cameras were positioned in groups of two. Targets near the center of the gore were seen by all four cameras, while targets near either end of the gore were only seen by two cameras. Although it would have been preferable for every area of the balloon be imaged by at least 3 cameras, only a total of four cameras were available for these tests. The cameras were equipped with ring flashes and wireless triggering devices. The camera triggering was staggered with an interval of 0.1 s. This avoided the flash from one camera causing glare in another camera's image. Since the balloon was stationary obtaining asynchronous images had no detrimental effect on measurement accuracy. An invar scale bar was used to set image scale. A second scale bar was used to assess the accuracy of the measurements. The balloon was inflated and the pressure monitored using an electronic pressure

gage. The balloon was inflated and images collected at gage pressures from 249 Pa to 4,828 Pa. Images were collected at every 689 Pa (0.1 psig).

C. 3 Meter Test Sphere Analytical Model

For the scale model test program, 16 gore spheres were fabricated and tested. The test article configuration included end caps at the pole locations. Fabric warp direction ran along the meridional direction while the fill ran along the hoop direction. Three planes of symmetry were used to model 1/8th of the full shape. Increased stiffness was modeled at the seam locations by appropriately increasing thickness in these areas. The commercial finite element program LS-Dyna was used to analyze the inflatable structure. Using the explicit finite element code helped to avoid some of the convergence difficulties associated with thin membrane structures. The dynamic relaxation option in LS-Dyna was used to obtain a quasi-static solution for each pressure level. The element formulation used was the Fully Integrated Belytschko-Tsay Membrane. There were a total of 3628 elements in the model. The finite element model mesh is shown in Fig. 10. The initial shape was determined using the photogrammetry measurements recorded for the lowest practical inflation pressure. A CAD model of the initial surface shape was constructed employing the symmetry conditions assumed in the model. The nodes of the finite element grid were projected onto this surface to achieve an accurate match. The non-linear orthotropic fabric option (LS-Dyna MAT_034) was used. See the results section for the specific details concerning the material property input data.

IV. Results

A. Bi-Axial Fabric Testing

The result of torsion cylinder testing of the two samples is shown in Fig. 11. It can be seen from the results that the influence of inflation pressure on shear stiffness for this fabric is not significant in the tested range. Therefore, an average value of 0.268 GPa was used for the fabric shear modulus in the FEA. These results and all others were calculated using an effective thickness of 0.0914 millimeter. It is assumed in the test data reduction and in the analysis that thinning is not present.

Figure 12 shows the results of the uni-axial strip tensile testing. The data indicates an initial non-linear region that transitions to a extended linear region. Based on results from balloon inflation testing, the region of interest is 0 to 4% in the fill direction and 0 to 2% in the warp direction. The presence of material creep at higher balloon inflation loads limited our investigation to this region.

After bi-axial testing, data reduction was completed to calculate apparent Young's Modulus in warp & fill directions. Additionally, the two Poisson's ratios, ν_{fw} & ν_{wf} , must be determined. Calculations were made at each of the different 1:1 load levels evaluated. The following system of equations was used to solve for the four unknowns:

$$\Delta \varepsilon_f = \frac{\Delta \sigma_f}{E_f} - \nu_{wf} \frac{\Delta \sigma_w}{E_w} \quad (1)$$

$$\Delta \varepsilon_w = \frac{\Delta \sigma_w}{E_w} - \nu_{fw} \frac{\Delta \sigma_f}{E_f} \quad (2)$$

In these equations, $\Delta \sigma_w$, $\Delta \sigma_f$, $\Delta \varepsilon_w$, and $\Delta \varepsilon_f$ are measured increments of stresses and strains in warp and fill directions, respectively. Figures 13 and 14 show plots of the bi-axial modulus measurements versus the load that they were measured at. Also included in these plots is a comparison with the uni-axial results. Figure 15 show plots of the Poisson's ratio measurements versus load state.

The bi-axial modulus testing was seen to under predict the actual material stiffness. This result was most notable for the bi-axial measurements made at lowest load. The measurement error was made clear when compared against the stiffer material response from the photogrammetric measurements of the inflated balloon. To investigate the measurement errors in the bi-axial testing, the horizontal load cell data was reviewed. There were observed differences between the two load cells used in the horizontal line of action. These in line load cells should in theory read the same value. Although the magnitude of the difference was as high as 6% in some cases, these differences were not significant. When fitting a curve to the horizontal load cell data, the R-Squared for one of the two cells was consistently lower. One cell gave consistently reasonable fits with R-Squared between 0.90 and 0.99. The

other cell contained a great deal of scatter with R-Squared in the 0.20 to 0.90 range. Modulus results were recalculated using only the load readings from the more consistent load cell. This exercise resulted in only small changes to the original modulus estimates. Although the error source was not pin pointed, the following improvements are suggested for the device.

- 1) Use higher density of load states where bi-axial measurements are taken
- 2) Greater number of overall samples
- 3) Improved weight relief for horizontal sample clamps
- 4) Use regression estimates for change in horizontal force
- 5) Replace horizontal load cells
- 6) LVDT instrumentation to track linear bearings controlling the sample center
- 7) Projection of laser alignment markings onto sample to ensure sample alignment

In the discussion of the structural analysis results, simulations are presented for two cases. The first case presents results using uni-axial data for warp and fill modulus. An evaluation of the bi-axial modulus at higher load states is then presented. For this second case, the uni-axial modulus results are used for the initial region and the bi-axial measurements are used for stress states higher than 15 MPa.

B. Photogrammetry Results and Strain Measurement

The pressure at 249 Pa was used as the baseline for determining the distance between targets. At this pressure the near spherical shape of the balloon was defined, yet the skin was subjected to minimal tension. It was not practical to obtain images of the balloon skin in an un-inflated state to obtain the true zero stress state of the balloon. At each pressure a set of three dimensional coordinates was obtained from the photogrammetric analysis. The distance between adjacent targets at each pressure was determined from the coordinates using,

$$L_r = \sqrt{(x_j - x_i)^2 + (y_j - y_i)^2 + (z_j - z_i)^2} \quad (3)$$

and

$$\Delta L_r = L_{r,\text{inflated}} - L_{r,\text{baseline}} \quad (4)$$

Comparing identical targets in inflated and baseline data sets the strain was obtained using,

$$\varepsilon_r = \frac{\Delta L_r}{L_r} \quad (5)$$

Because the accuracy of any photogrammetric analysis is dependent on camera placement it is necessary to assess accuracy for each project. For this study we used two invar scale bars. The first bar was 1596 mm in length and was used to set the scale of the images. A second 1346 mm invar bar was used to assess the overall accuracy of the measurement system. Table 1 compares the measured length of the bar for each data set. The data indicates that the all measurements fall within 0.1 mm of the Mean.

Table 1. Comparison between actual and measured scale bar lengths

Pressure (gage, Pa)	Actual Length (mm)	Measured Length (mm)
249	1346.00	1345.82
689	1346.00	1345.65
1379	1346.00	1345.71
2068	1346.00	1345.75
2758	1346.00	1345.81
3447	1346.00	1345.74
4137	1346.00	1345.67
4848	1346.00	1345.68
	Mean	1345.73
	St. Dev.	0.06

In addition to the general understanding of strain, as in equation 5, the photogrammetry data enables a more detailed understanding of the strain state. Using the shape measurements at the minimal inflation load of 249 Pa established the reference configuration or material coordinates \mathbf{X} . The mapping x is used to describe the motion as

pressure load is applied. A particle of material initially at position \mathbf{X} in reference coordinates, moves to a position \mathbf{x} in spatial coordinates. Displacement is expressed as the difference between the spatial and reference coordinates.

$$\mathbf{x} = x(\mathbf{X}, t) \quad (6)$$

$$\mathbf{u}(t) = \mathbf{x}(t) - \mathbf{X} \quad (7)$$

Using indicial notation the Lagrangian strain tensor can be expressed as the following.

$$E_{AB} = \frac{1}{2} \left(\frac{\partial u_i}{\partial X_A} \frac{\partial u_i}{\partial X_B} + \frac{\partial u_B}{\partial X_A} + \frac{\partial u_A}{\partial X_B} \right) \quad (8)$$

Some Mathematica code was developed to calculate the Lagrangian strain tensor given the photogrammetry data sets. The scale bars provided for the definition of a fixed reference coordinate system. Sorts were conducted to put the data in the structured i,j grid used for the retro targets. In the main loop, the following steps were followed for each material coordinate.

- 1) Establish x,y local coordinate system using the structured i,j target grid
- 2) Transform material and current coordinates into local system
- 3) Calculate displacements in local coordinate frame
- 4) Estimate partial derivatives
- 5) Calculate strain tensor components

These results were compared with the general approach used in equation 5 and as expected the results were in very close agreement. An example of the resultant strain field is shown in Fig. 16. Using some vector algebra an approximate balloon center could be estimated. This enabled displacement field plots relative to the estimated balloon center coordinate system. Figure 17 shows an example of the displacement field plot.

C. Structural Analysis Model

Structural analysis results are presented for two cases. The first case investigates the uni-axial modulus measurements. Analysis runs using the uni-axial modulus measurements are compared with the photogrammetry results of the balloon inflation experiment. The second case investigates the bi-axial modulus measurements at load states beyond the first two measurements. So for the eight total bi-axial modulus measurement points, the third through the eighth are used in this case. Analysis runs for this case are also compared with the photogrammetry results of the balloon inflation experiment.

As mentioned in the discussion of the material testing results, the bi-axial modulus measurements at low loads appeared to be significantly less than the actual observed stiffness. It was expected that the bi-axial results wouldn't exactly match the uni-axial results. This difference was not expected to be very large. As shown in Figures 13 and 14, the first two bi-axial measurement points deviated from the uni-axial data by as much as 50%. The density of measurement points in this low load region was also insufficient. The uni-axial data showed significant modulus change in the low load region. There were not enough data points to determine if the bi-axial measurements exhibit the same trend. These two observations help to show that the bi-axial modulus predictions in the low load regions were not accurate. To confirm this observation a structural analysis model was run using the as measured bi-axial modulus predictions. When compared against the inflated balloon experiment, the difference in strain between the analysis model and photogrammetry measurements was as high as 60%. The largest difference was observed at the lowest measured load. The difference between the model and experiment dropped as the inflation loads increased. The modulus measurements at low load were not accurate, but some further investigations were possible to evaluate the bi-axial measurements at higher load states.

As expected, there appeared to be some level of agreement between the uni-axial tensile testing and the photogrammetry results for the inflated balloon. Structural models were run to report these comparisons for all six of the inflation load measurements that have been reported for the photogrammetry experiment. In this run the engineering constants for the material were taken from the following:

- 1) Uni-Axial Test - E_f & E_w
- 2) Bi-Axial Test - ν_{fw} & ν_{wf}
- 3) Torsion Cylinder Test – Shear modulus

Results are presented in Fig. 18 through 20 for hoop and meridian strain. In these graphs the gore centerline strains are reported at different elevations, as measured from the equator plane. The material fill direction coincided with

the hoop direction for the balloon experiment. Using strain at the equator as a reference, the model versus experiment difference for hoop strain was between 5 and 14% for the three cases. The materials warp direction coincided with the meridian direction for the balloon experiment. The model versus experiment difference for meridian strain was between 15 and 33% for the three cases. Using the modulus from uni-axial experiments over predicts stiffness in both warp and fill directions. For this specific material and load condition, the warp over predicts stiffness by a greater margin than the fill.

In order to get a general assessment of bi-axial modulus measurements at higher loading, a hybrid case was investigated. In this run the engineering constants for the material were taken from the following:

- 1) Uni-Axial Test - E_f & E_w at loads less than 15 MPa
Bi-Axial Test - E_f & E_w at loads greater than 15 MPa
- 2) Bi-Axial Test - ν_{fw} & ν_{wf}
- 3) Torsion Cylinder Test – Shear modulus

It was not possible to evaluate the warp direction bi-axial measurements with this case. With the warp's higher stiffness, all the cases through 4579 Pa did not extend beyond the 15 MPa load region. With the baseline material thickness, the 15 MPa load is equal to 137 N/cm. In the case of the fill direction, the material response extended beyond the 15 MPa region. This provided several points where the bi-axial fill modulus measurements could be evaluated. The load case of 1820 Pa inflation pressure was taken as a baseline. Strain increment versus load increment was compared with the experimental data. Figure 21 shows plots of strain increment versus elevation, as measured from the equator plane. The data is presented is for four delta pressure conditions of; 690, 1380, 2070, and 2760 Pa. Using the hybrid case and evaluating strain increments, the bi-axial measurements of modulus above the 15 MPa initial region are in good agreement with the Photogrammetry experimental measurements.

V. Conclusion

Material stiffness values determined from uni-axial testing were stiffer than the measured balloon response due to inflation loads. This result helps to illustrate the need for a bi-axial fabric testing device. There were mixed results when evaluating the stiffness predictions generated using the new bi-axial testing device. The bi-axial device was ineffective for load regions less than 137 N/cm. Bi-axial device design changes and experimental setup improvements have been identified to help rectify this problem. Six of the bi-axial fill modulus measurements were used to evaluate load regions greater than 137 N/cm. These fill modulus measurements showed much better agreement with the responses observed during balloon inflation testing. Additional evaluations of the new bi-axial device will be needed to validate its performance after the noted design improvements have been made.

The implementation of Photogrammetry was a critical aspect of this study allowing for a more detailed and rigorous evaluation of the bi-axial testing device. Deformation and strain are the key validation parameters for comparing model versus experiment results for inflatable fabric products. In the balloon inflation experiment, deformation was characterized by tracking the location of the targets at each load level. With the balloon deformation characterized, material strain versus load was compared with the material stiffness predicted from bi-axial testing. These strains, calculated using photogrammetry, provided a much more detailed data set for model vs. experiment correlation.

Acknowledgments

Joseph V. Welch thanks the University of Delaware Mechanical Engineering graduates who designed and fabricated the bi-axial device as part of their Senior Design competition. These individuals are Dan Gleeson, David Forney, and Jonathan Watts.

References

- ¹Poturi, P., Perez Ciurezu, D.A., Ramgulam R., "Measurement of meso-scale deformations for modeling textile composites," *Proceedings of the 2nd International Conference on Composites Testing and Model Identification CompTest 2004*, University of Bristol, Bristol, U.K., 2004.
- ²Rand, J.L., "Balloon Film Strain Measurement," *Advances in Space Research*, Vol. 3, No. 6, 1983, pp. 45-48, (BT-2470.06).
- ³Pappa, R.S., Geirsch, L.R., and Quagliaroli, J.M., "Photogrammetry of a 5-m Inflatable Space Antenna with Consumer-Grade Digital Cameras," *Experimental Techniques*, July/August, 2001, pp. 21-29.

⁴Jones T.W. and Pappa, R.S., "Dot Projection Photogrammetric Technique for Shape Measurements of Aerospace Test Articles," *Proceedings of the 40th AIAA Aerospace Sciences Meeting and Exhibit*, AIAA-2002-532, Reno, NV, 2002.

⁵Blandino, J.R., Johnston, J.D., and Dharamsi, U.K., "Corner Wrinkling of a Square Kapton Membrane," *Journal of Spacecraft and Rockets*, Vol. 39, No. 5, Sept-Oct, 2002, pp. 717-724.

⁶Blandino, J.R., Johnston, J.D., Miles, J.J., and Dharamsi, U.K., "The Effect of Asymmetric Mechanical and Thermal Loading on Membrane Wrinkling," *Proceedings of the 43rd AIAA/ASME/ASCE/AHS/ASC Structures, Structural Dynamics and Materials Conference*, AIAA-2002-1371, Denver, Colorado, 2002.

⁷Blandino, J.R., Sterling, J., Baginski, F., Steadman, E., Black, J.T., and Pappa, R.S., "Optical Strain Measurement of an Inflated Cylinder using Photogrammetry with Application to Scientific Balloons," *Proceedings of the 45th AIAA/ASME/ASCE/AHS/ASC Structures, Structural Dynamics and Materials Conference*, AIAA-2004-1500, Palm Springs, California, 2004.

⁸Baginski F., Schur W., "Structural analysis of pneumatic envelopes: Variational formulation and optimization-based solution process," *AIAA Journal*, Vol. 41, No. 2, 2003, pp. 304-311.

⁹Baginski F., Collier W., "A Mathematical Model for the Strained Shape of a Large Scientific Balloon at Float Altitude," *ASME Journal of Applied Mechanics*, Vol. 67, No. 1, 2000, 6-16.

¹⁰Diehl T., Dixon R.D., Lamontia M.A., Hanks J.A., "The Development and Use of a Robust Modeling Approach for Predicting Structural Performance of Woven Fabrics Using Abaqus," *Proceedings of the 2003 Abaqus Users' Conference*, ABAQUS Inc., Newport, Rhode Island, 2003.

¹¹Cavallaro P.V., Sadegh A.M., Quigley, C.J., Johnson A.R., "Effects of Coupled Biaxial Tension and Shear Stresses on Decrimping Behavior in Pressurized Woven Fabrics," Naval Undersea Warfare Center, Technical Report 11,571, Newport, Rhode Island, October 2004.

¹²Liu X., Jenkins C.H., Schur W., "Large deflection analysis of pneumatic envelopes using a penalty parameter modified material model," *Finite Elements in Analysis and Design*, Vol. 37, 2001, pp. 233-251.

¹³Tabiei, A., Ivanov, I., "Computational micro-mechanical model of flexible woven fabric for finite element impact simulation," *International Journal for Numerical Methods in Engineering*, Vol. 53, 2002, pp. 1259-1276.

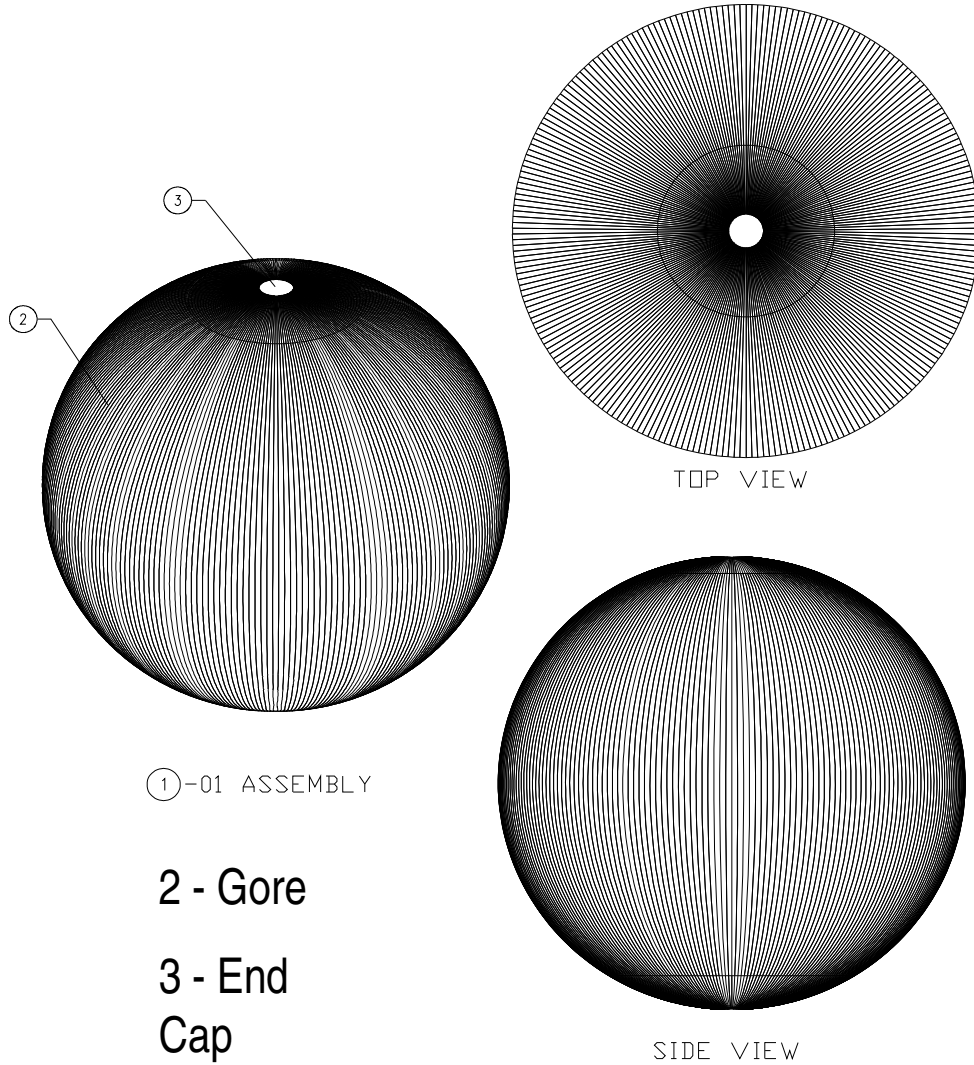


Figure 1. Design concept proposed for Alternate ULDB.

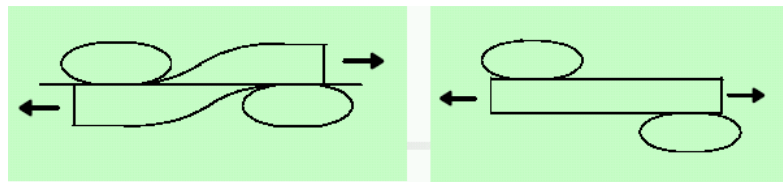


Figure 2. Uni-axial strip tensile movement of yarns.

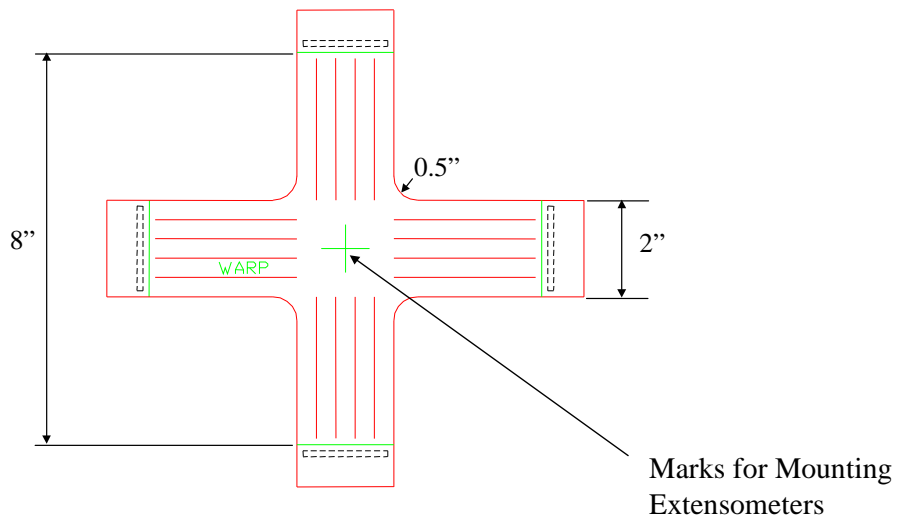


Figure 3. Cruciform fabric test sample.

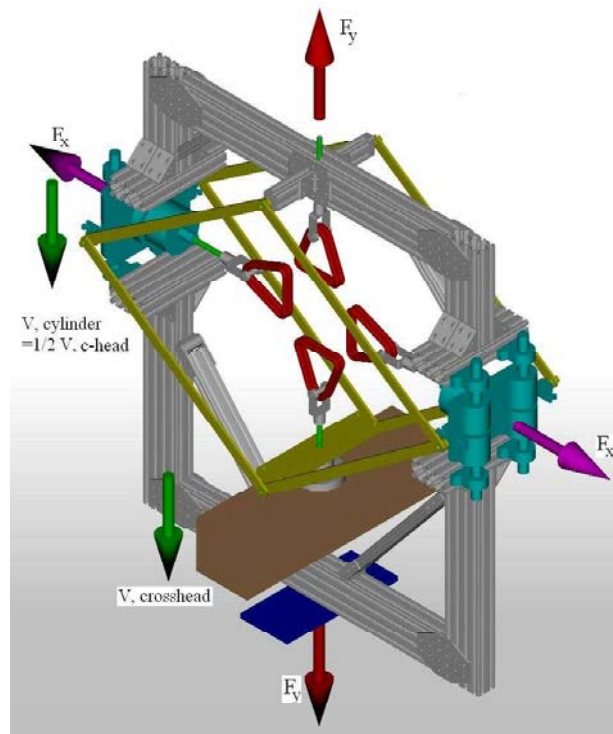


Figure 4. Bi-axial load apparatus CAD model.



Figure 5. Bi-axial test device installed in Instron.

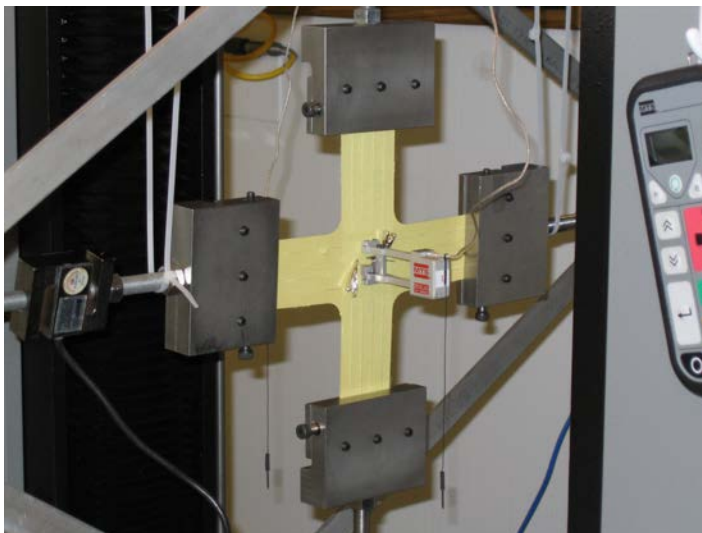


Figure 6. Cruciform sample loading.

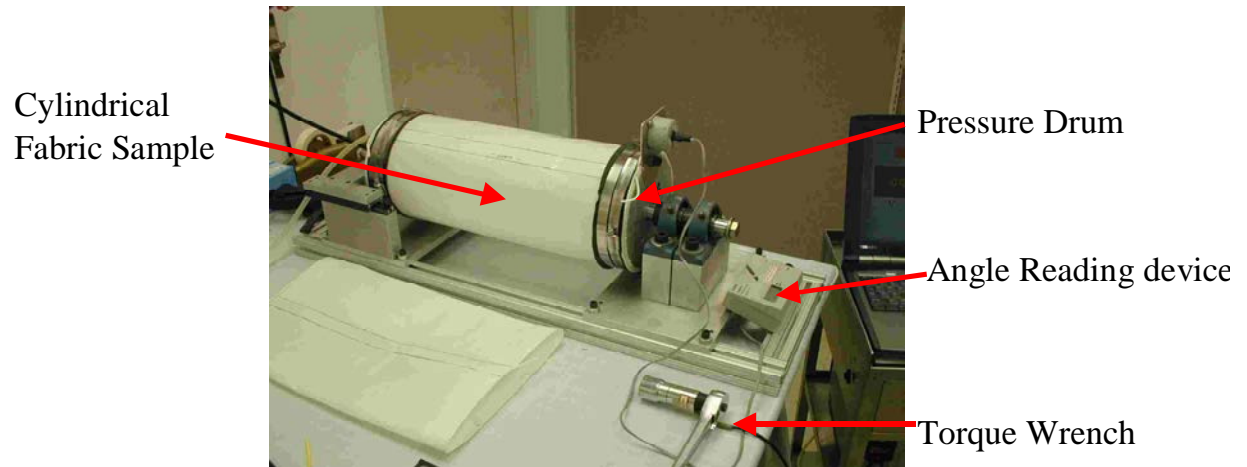


Figure7. Inflated cylinder torsion test.



Figure 8. Balloon with retro-reflective targets.



Figure 9. Camera positions with respect to the balloon.

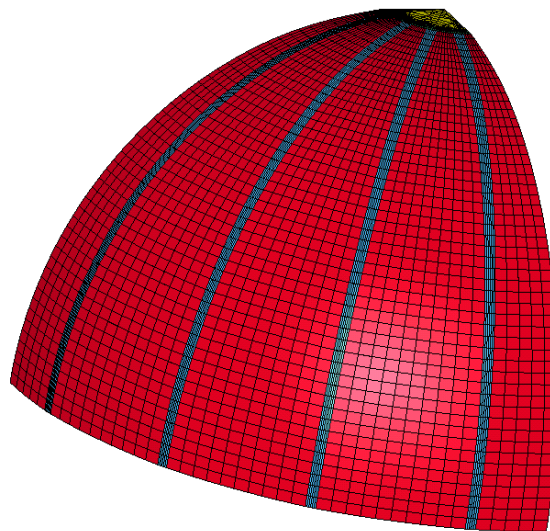


Figure 10. Finite element model mesh.

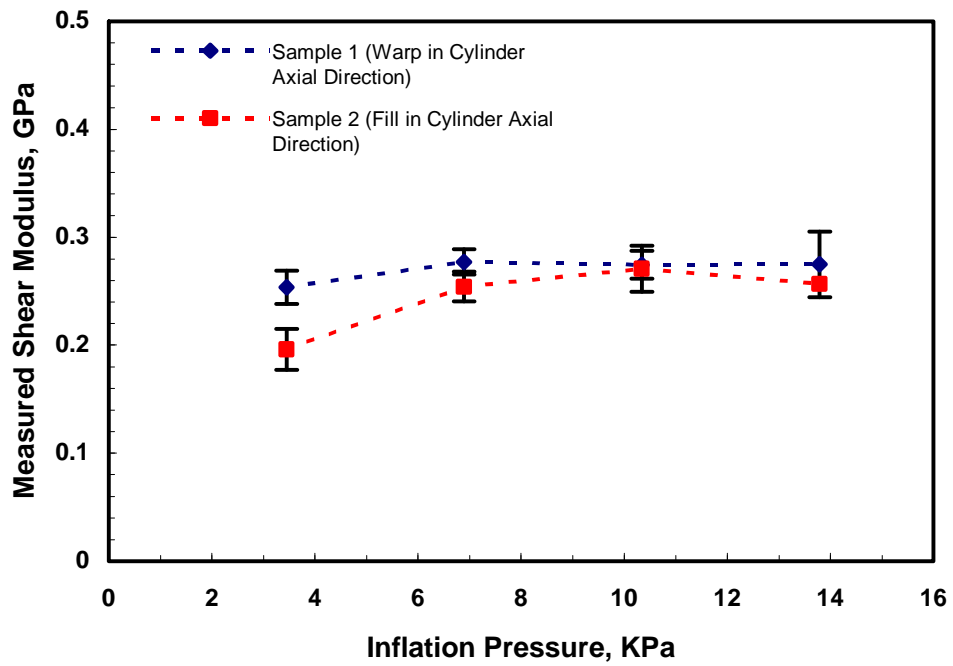


Figure 11. Shear modulus measurements.

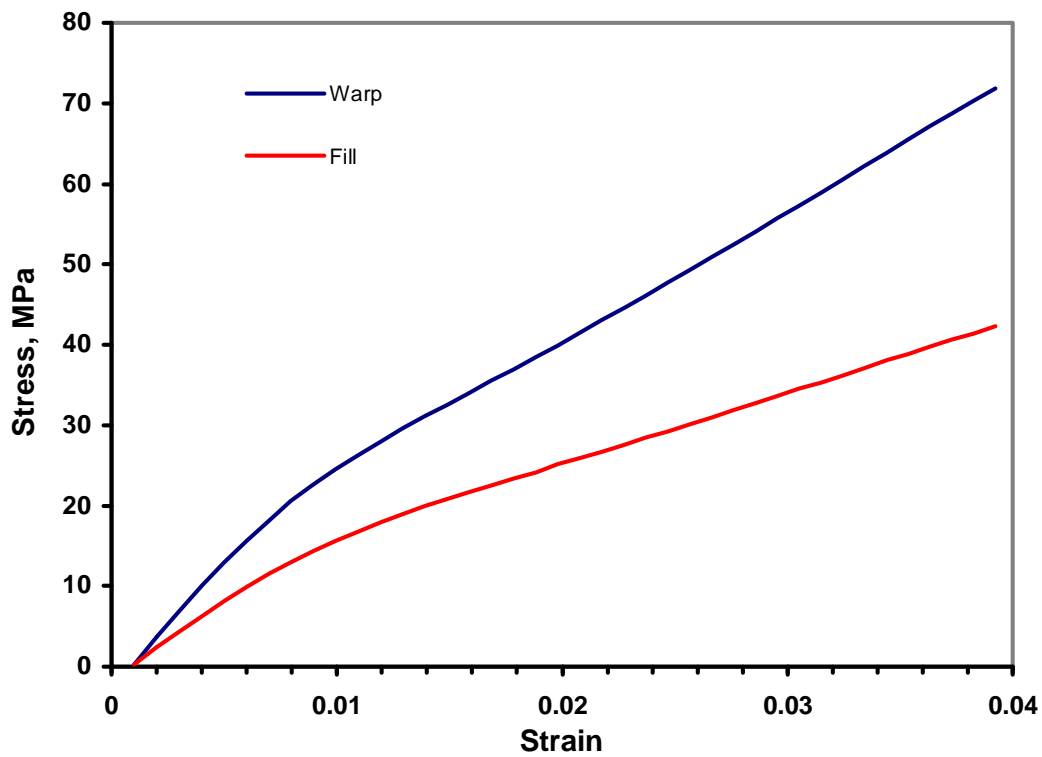


Figure 12. Uni-axial stress-strain curve.

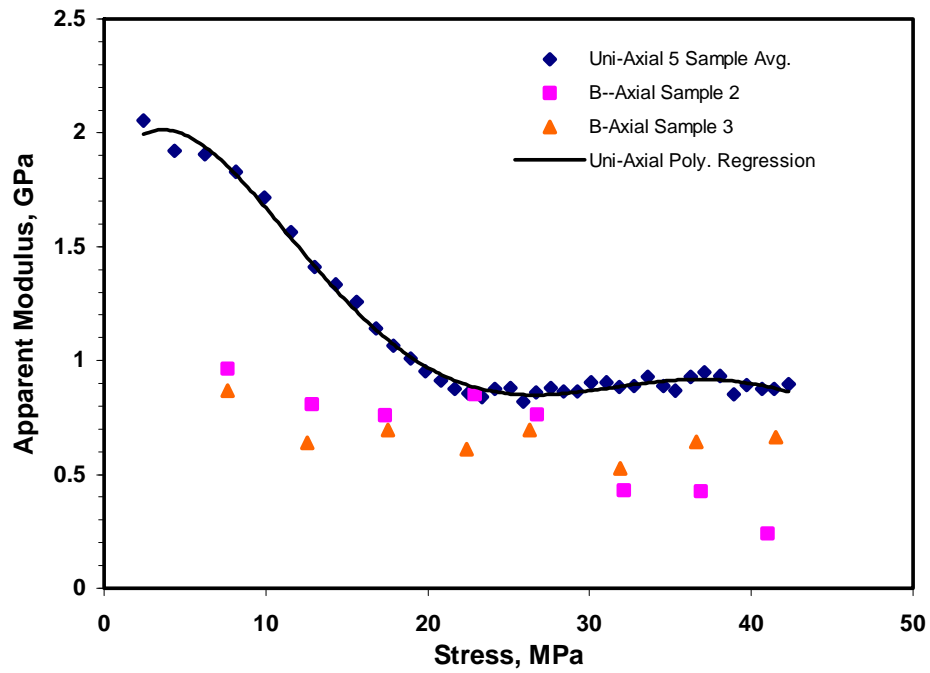


Figure 13. Fill direction modulus measurements.

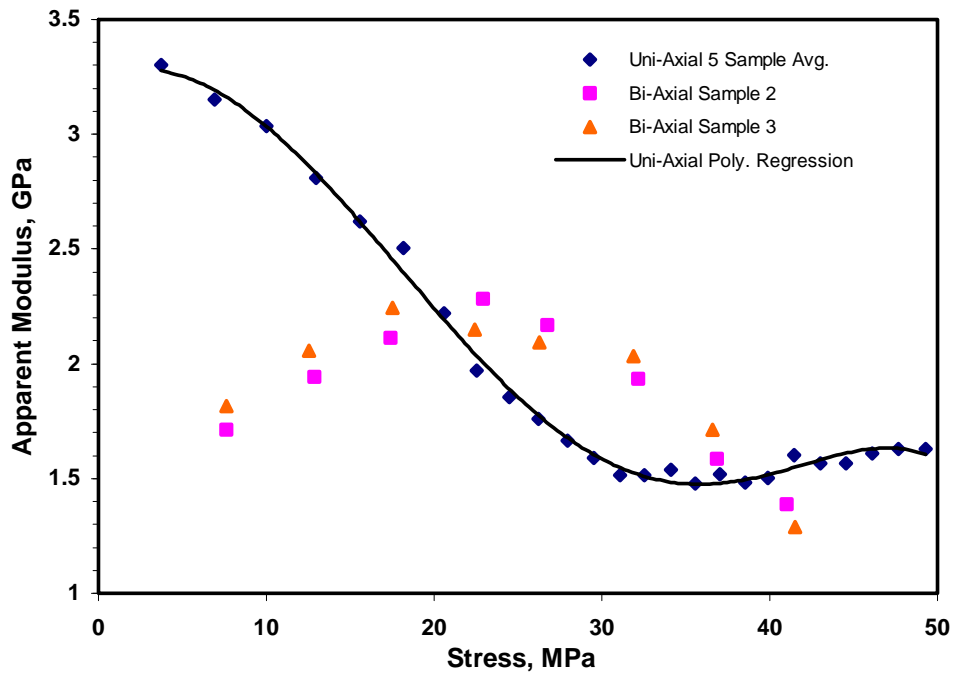


Figure 14. Warp direction modulus measurements.

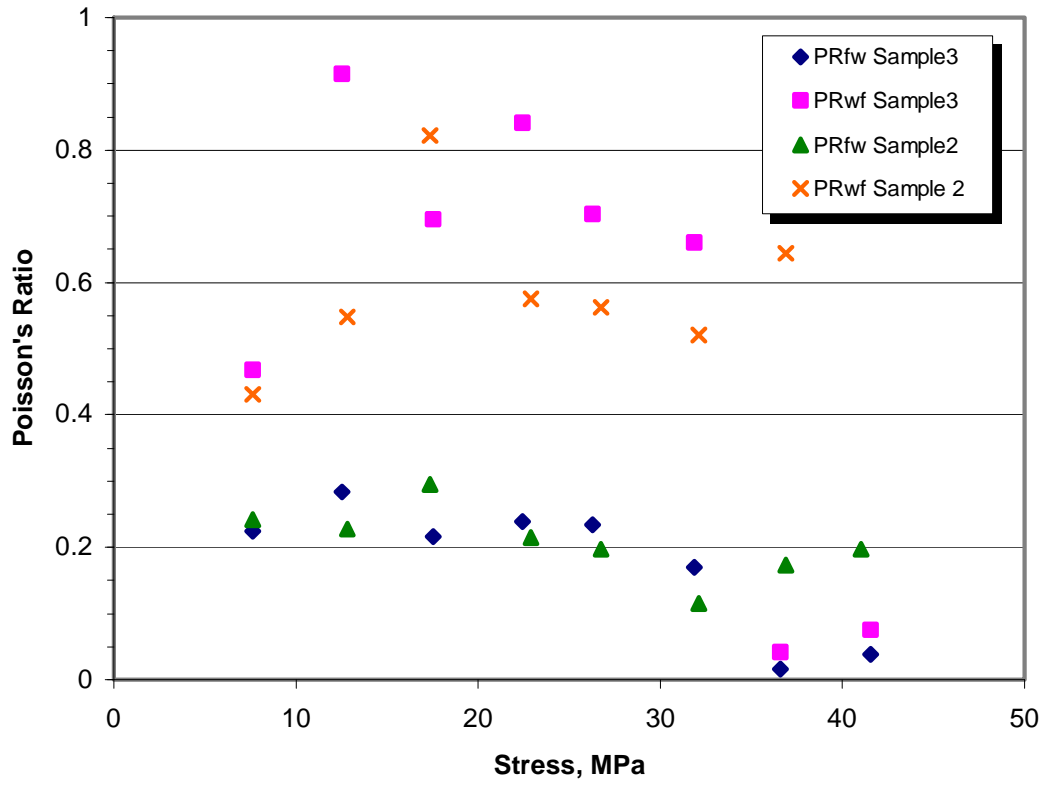


Figure 15. Measured Poisson's Ratio.

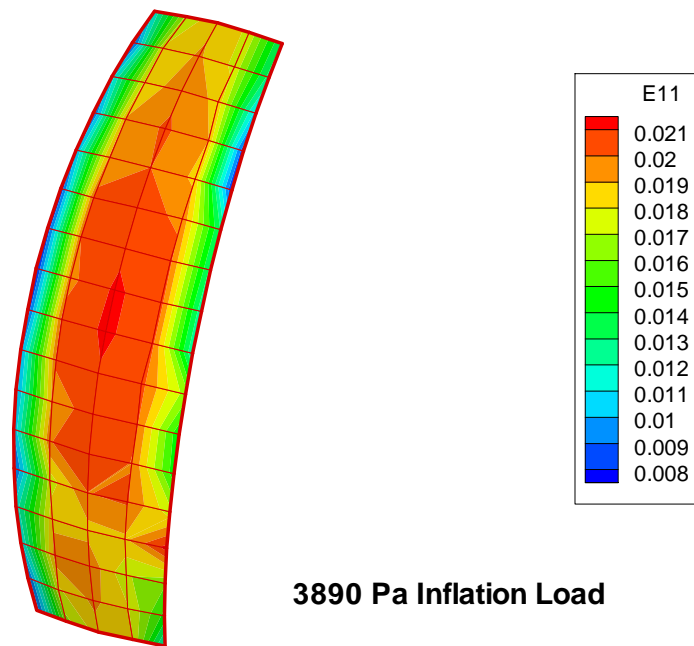


Figure 16. Hoop direction strain contour plot (experiment)

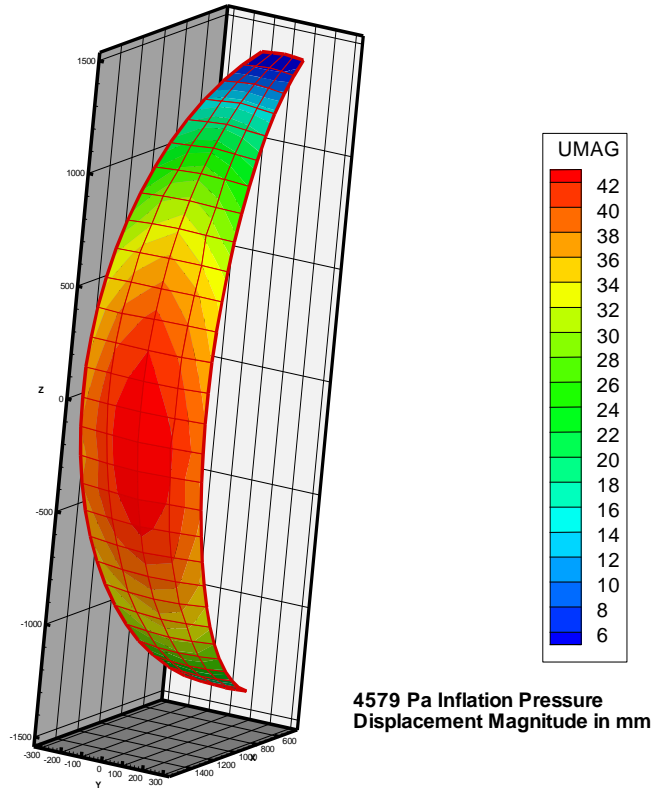


Figure 17. Displacement magnitude contour plot (experiment)

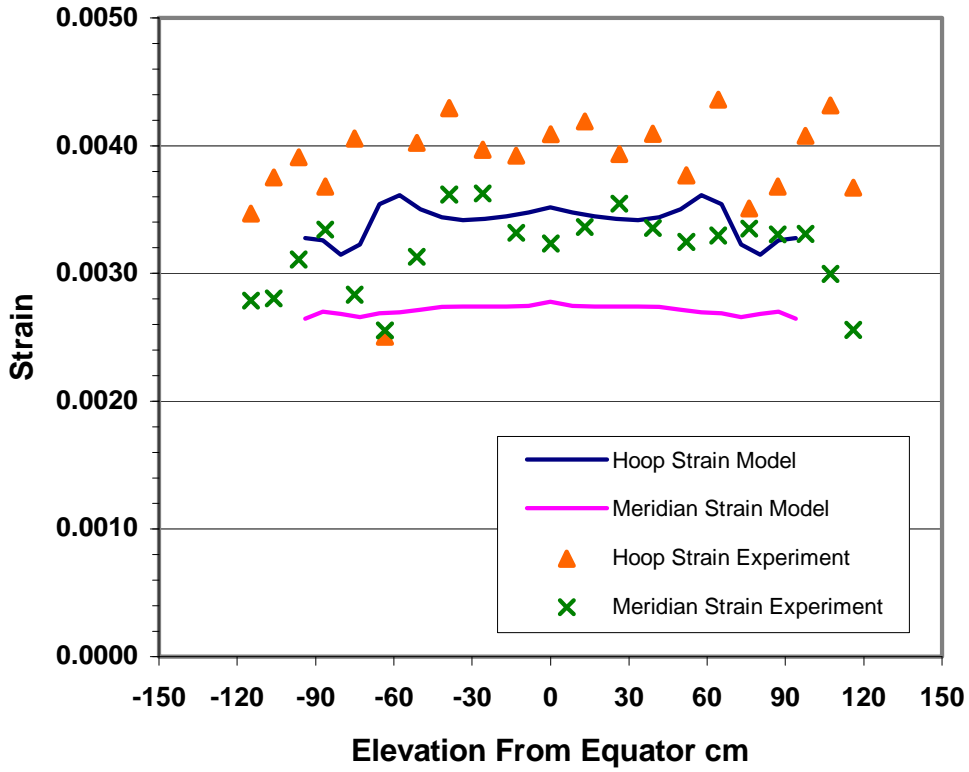


Figure 18. Hoop and meridian strain along gore centerline at 1131 Pa.

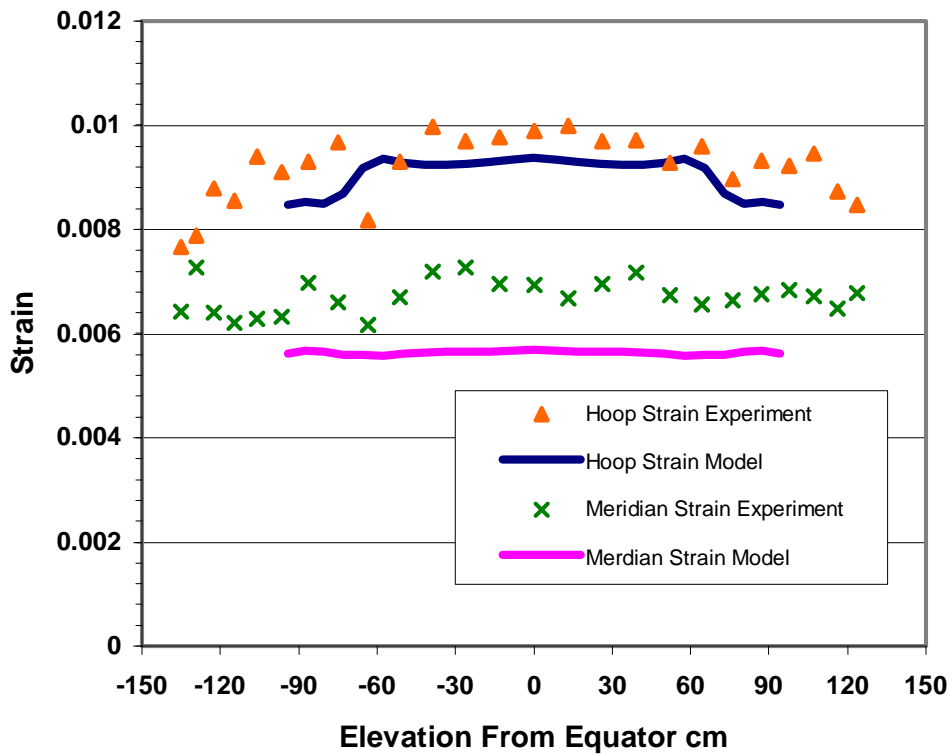


Figure 19. Hoop and meridian strain along gore centerline at 2510 Pa.

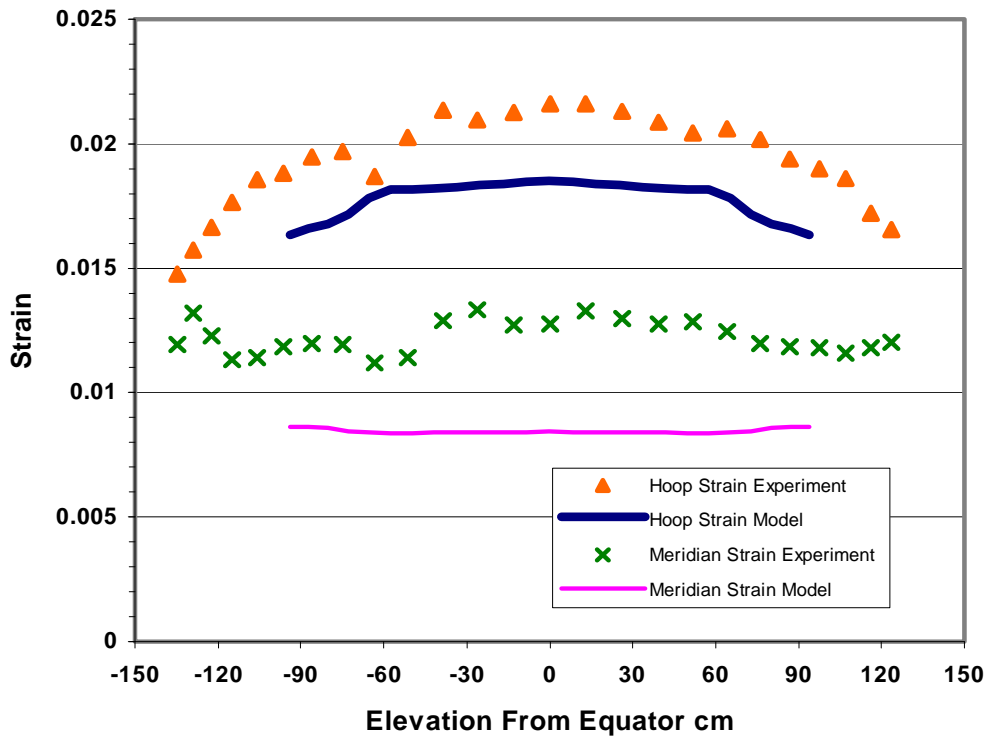


Figure 20. Hoop and meridian strain along gore centerline at 3890 Pa.

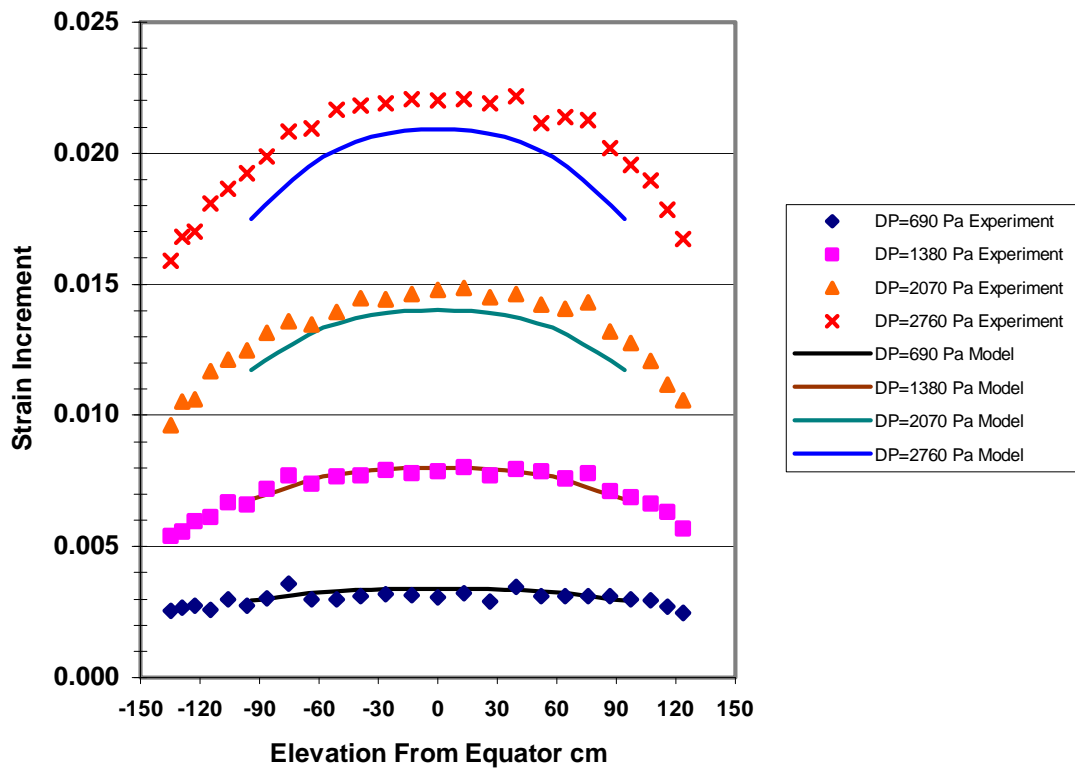


Figure 21. Strain increment using bi-axial modulus measurements